Network Polymers incorporating Lipid-Bilayer Disrupting

Polymers: Towards Antiviral Functionality

Kevin M. Burridge,^a Monica S. Rahman,^a Nethmi De Alwis Watuthanthrige,^a Emma Gordon,^a

Muhammad Zeeshan Shah, a Bhagya Madhushani Chandrarathne, a Gary A. Lorigan, Richard C.

Page,^{a*} Dominik Konkolewicz^{a*}

^a Department of Chemistry and Biochemistry, Miami University, 651 E High St, Oxford, OH

45056, USA

† Corresponding Authors: RCP: pagerc@miamiOH.edu, DK: d.konkolewicz@miamiOH.edu

Abstract:

Designing a surface that can disinfect itself can reduce labor-intensive cleanings and harmful

waste, and mitigate spread of surface borne diseases. Additionally, since COVID-19 being an

airborne pathogen, surface modification of masks and filters could assist with infection control.

Styrene-maleic acid (SMA) copolymers and their derivatives were shown to have lipid-bilayer

disrupting properties, making them candidates as anti-viral materials. A series of network

polymers with styrene-maleic acid-based polymers and control over polymer chain-length and

composition were synthesized. All the polymers formed mechanically robust structures, with

tunable Young's moduli on the order of MPa, and tunable swelling capability in water. The SMA-

based bulk materials, containing a zwitterionic polar unit, showed excellent lipid disrupting

properties, being up to 2 times more efficient than a 10% triton solution. The highest performance

was observed for materials with lower crosslink density or shorter chain-lengths, with lipid

disruption capability correlating with swelling ratio. Additionally, the material can capture the spike protein of SARS-CoV-2, with up to 90% efficiency. Both the lipid disrupting and spike protein capture ability could be repeated for multiple cycles. Finally, the materials are shown to modify various porous and non-porous substrates including surgical and KN95 masks. Functional network modified masks had up to 6 times higher bilayer disruption ability than the unmodified masks without inhibiting flow.

Introduction:

One of the timeless ways in which infectious diseases are controlled is by the treatment of human environments rather than the much more complicated matter of the treatment of the infected. Household cleaning products kill 99.9% of surface pathogens for the price of pennies per square meter.¹⁻⁴ The next natural step is to design a surface that disinfects itself, which could reduce the spread of surface borne diseases.^{5,6} Furthermore, with COVID-19 being a primarily airborne pathogen, designing anti-viral and self-disinfecting materials that can attach to air filters may be one of the most effective environmental controls.⁷⁻¹⁰

Prior efforts in designing in disinfecting materials has focused primarily on bacterial pathogens, with substantially fewer studies on antiviral materials.^{11–15} Some antimicrobial principles are effective against both bacteria and viruses, such as copper^{16,17} or silver¹⁸ on a surface. Small molecule inhibitors can also be loaded into a material, but usually they must be noncovalently bound to function and are eventually washed away.^{19–21} Thus, surface-bound polymers such as lipid-bilayer disrupting and protein-capturing macromolecules are promising antimicrobial and anti-viral agents, due to their potential to be used over a longer timeframe.

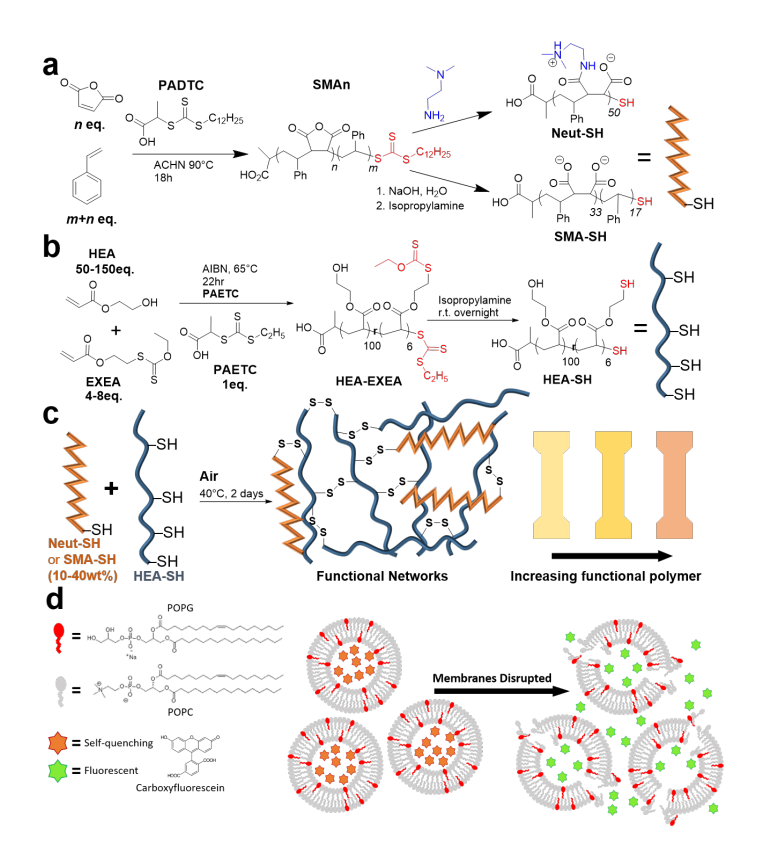
Polymeric materials have been designed to interact with viruses and environments where viruses are present. At the simplest level, polymers are used as physical barriers though personal protective

equipment such as gloves, masks, etc.²² However, modern polymer chemistry has also enabled macromolecular materials that either capture viral particles or surface exposed viral proteins. Taking advantage of the hydrophobicity and anionic charge of the SARS-CoV-2 spike protein could lead to efficient capture and immobilization on hydrophobic and cationic polymers.²³ Similarly, cationic and hydrophobic materials have been shown to inactivate influenza.^{24,25} Further, using a library of polymer functionalities in a combinatorial microarray manner can lead to surfaces with the ability to capture virus like particles, facilitating eventual detection and identification.²⁶

As an alternative pathway to protein capture, disrupting the viral lipid envelope, present in many pathogenic viruses, is an alternative and complementary approach to environmental sanitation and prevention of viral transmission.²⁷ Further, the antiviral activity for macromolecular surfactants and bilayer disrupting polymers, such as polymeric quaternized amines (pQA) has been demonstrated. The activity of pQAs involves disruption of phospholipid membranes, with pQA materials being active against the enveloped influenza virus, but not poliovirus, which is not enveloped.28 Similarly, quaternized polyethylenimine29 is an effective antiviral coating. The mechanism of action for quaternary ammonium based surfactants has been thoroughly explored,30 and applied to create antimicrobial and virucidal modified fibers through a grafting of the quaternary ammonium group to existing N95 masks.³¹ While effective for disruption of viral membranes, pQA polymers are susceptible to biofouling by irreversibly binding viral proteins.³² Polymers deviating from the purely cationic formulations have also been investigated, such as those incorporating a sulfonated block which disrupts negatively charged membranes by promoting a highly acidic environment.33 The antiviral activity of polyacrylic acids, polymethacrylic acids, and other polyanions has been known for decades.³⁴ However, the water solubility of these polymers and their highly ionic characteristics can limit their widescale utility or attachent to all surfaces.

Styrene-maleic acid (SMA) copolymers and their derivatives are promising candidates for antimicrobial applications due to their intrinsic interactions with lipids and the ease with which the parent anhydride (SMAn) functionality can be manipulated.^{35–39} The lipid interacting character arises from the high cross reactivity of the component monomers in radical polymerization, which results in the pre-polar anhydride group alternating with the nonpolar styrene residues.^{40–45} Polymerization performed with an excess of styrene relative to maleic anhydride results in a homostyrene tail after the alternating region. While prior work on SMA-based antimicrobials has been focused on bacteria,^{46–49} the mechanism of membrane disruption should be applicable to enveloped viruses such as SARS-CoV-2.⁵⁰

Inspired by the demonstrated effectiveness of lipid interacting polymers and the utility of SMA, this work set out to develop membrane-disrupting polymer networks that incorporated, by disulfide bridges, either SMA (in the form of SMA-SH) or a zwitterionic tertiary amine derivative of SMAn (Neut-SH) (Scheme 1). SMA-based polymers were synthesized by reversible addition-fragmentation chain transfer (RAFT) polymerization, ⁵¹⁻⁵⁹ which affords low-dispersity polymers of predefined chain lengths and high end-group fidelity. This enables precision design of polymer materials, both at the network structure level and also at the level of the macromolecule. Combining these two together gives a unique strategy for designing materials with the capacity of robust mechanical properties, adhesive capability and potential antiviral characteristics. These potent antiviral materials with excellent mechanical and adhesive properties could be attached to existing high contact substrates and filter materials. This can lead to a dual approach to the reduction of viral transfer: surface modification can potentially inhibit the infection cycle of viruses that undergo fomite transmission, ^{6,60,61} and mask materials can be functionalized to reduce transmission of airbone viruses such as SARS-CoV-2.⁶²



Scheme 1. Synthesis of a) functional polymers Neut-SH and SMA-SH; b) scaffold polymers HEA-SH; and c) functional networks. The Neut-SH is the derivative of SMAn with 1:1 styrene:maleic anhydride and no styrene tail. The SMA-SH is the derivative of SMAn with 1.5:1 styrene:maleic anhydride ratio and as a result has a short styrene tail. d) Mechanism of fluorophore encapsulation/release experiment. At first, high localized concentrations of liposome-encapsulated fluorophore are self-quenching and decrease quantum yield. Upon disruption of the liposomes, fluorophore is released into bulk solution, diluting the previously localized concentrated populations, resulting in increased fluorescence.

Results and Discussion

Thiol-disulfide chemistry was used in network synthesis, due to the intrinsic compatibility between RAFT based polymers and thiol chemistry, 63 and the simplicity of the crosslinking

process, requiring only ambient molecular oxygen to drive the crosslinking process. The trithiocarbonate-based RAFT chain transfer agents (CTA) on both the backbone forming polymer and the SMA-based polymers can be transformed into free thiols by aminolysis, which eventually form disulfide bridges on exposure to air (Scheme 1a). The network polymers which formed the scaffold for these functional polymers were RAFT-synthesized copolymers of hydroxyethyl acrylate (HEA) and protected thiols in the form of ethylxanthate ethyl acrylate (EXEA) (Scheme 1b). The EXEA monomers were aminolyzed along with the CTA to reveal free thiols for crosslinking and binding of functional polymers (Scheme 1c). Typically this crosslinking process occurs over several hours, although the free thiol polymers should not be stored for extended periods of time, such as days or weeks, to avoid disulfide formation in unintended structures. A series of chain length and crosslinker densities of the network polymers were synthesized to assess the effects of network stiffness on activity (Table S2).

To assess the membrane-disrupting activity of these networks, a fluorophore encapsulation/release assay was used (Scheme 1d).⁶⁴ The membrane-impermeable fluorophore 5(6)-carboxyfluorescein is first encapsulated at high concentration within liposomes of approximately 100 nm. Inside the liposomes, the fluorophore self-quenches. When the lipid-bilayer is disrupted, the encapsulated fluorophore is released, causing an increase in fluorescence.⁶⁵ Liposomes were composed of 1-palmitoyl-2-oleoyl-sn-glycero-3-phosphocholine (POPC), and 1-palmitoyl-2-oleoyl-sn-glycero-3-phosphoglycerol (POPG), at a ratio of 9:1 POPC:POPG, which closely approximates the fluidity and charge composition of the mammalian membranes from which the viral envelope is derived.^{66,67} Figure 1a shows that the HEA/EXEA polymers were synthesized with good control over molecular weight and dispersity (Table S3), with minor high-MW shoulders due to some

deprotection and coupling of xanthate-protected thiols, or conventional radical combination. While the observed M_n values are all slightly higher than M_{n,th}, dispersities are low (≤1.3). Figure S1 confirms that the SMA based polymers were well controlled. ¹H NMR of polymer solutions and IR spectra of the network materials are in Figure S2 and S3. IR spectra indicate that the SMA and Neut functionalities are present, due to the disappearance of anhydride peaks at 1800 cm^{-1,68} Further, the HEA/SMA or HEA/Neut materials being a blend of the individual IR spectra. Mechanical testing of the materials revealed that, as expected, higher chain lengths and crosslink densities resulted in higher Young's moduli, with a dramatic shift in stiffness moving from DP100 to DP150 and from a crosslinker density of 6% to 8% as relative to the central 100/6 HEA material (Figure 1b-c). Finally, figure 1d shows that the addition of 20% functional polymer does not adversely affect the material stiffness, with comparable Young's moduli across 100/6 HEA and 100/6 20% SMA and 100/6 20% Neut. Fracture energies for several materials were also collected (Figure S4) and correlated well with Young's moduli. Once again the 100/6 20% Neut material exhibited comparable fracture toughness compared to the 100/6% HEA.

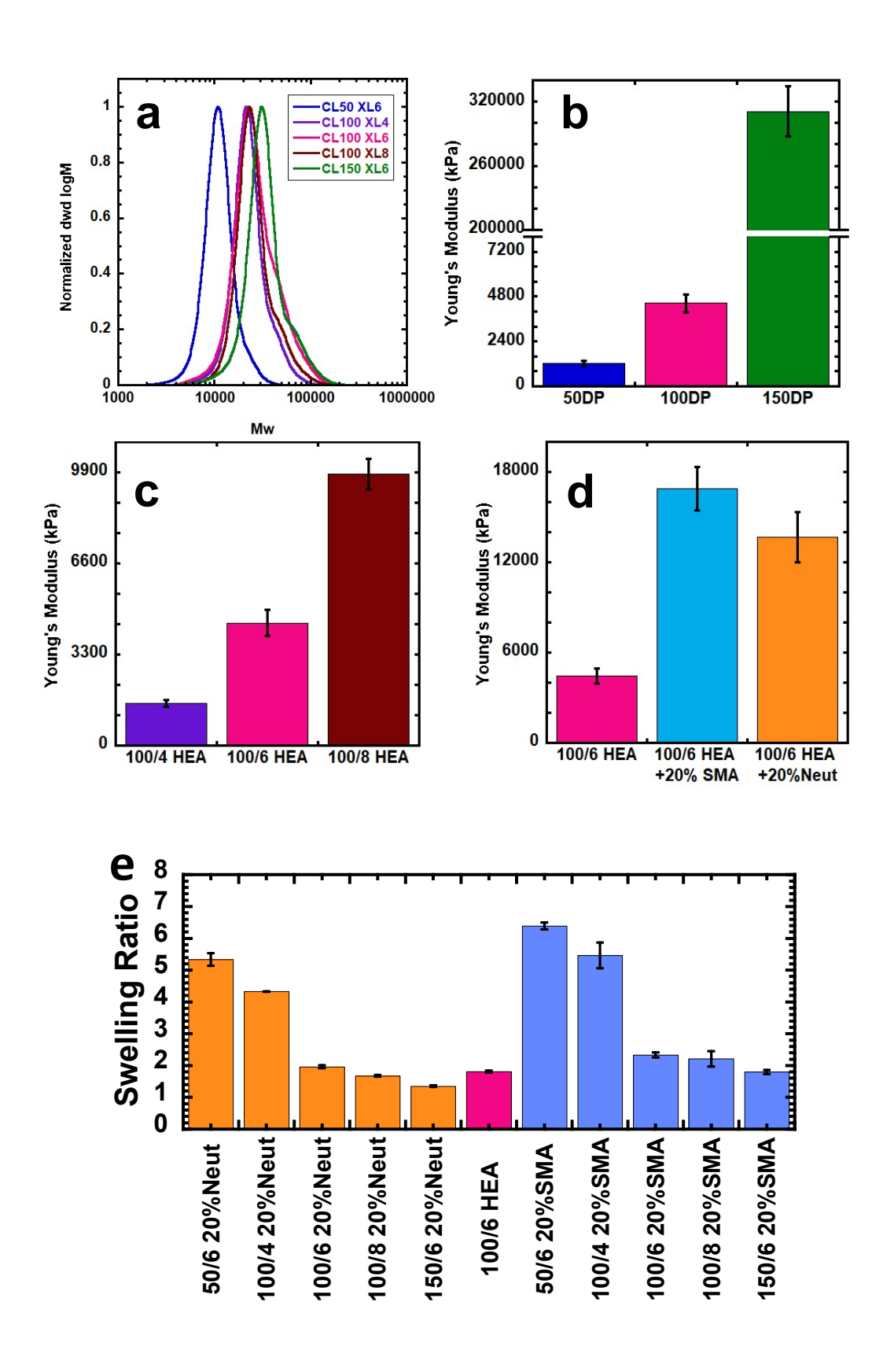


Figure 1. (a) SEC results of varying chain length and crosslinker densities for HEA network polymer. (b-d) Young's modulus of materials of varying (b) network polymer chain length, (c) crosslinker density, and (d) functional polymer content (e) Swelling ratios of Neut and SMA containing networks of PHEA networks.

The materials displayed glass transition temperatures varying from 8-40 °C (Table S4, Figure S5-S9) and good thermal stability in the range of 30-400 °C (Figure S10). Additionally, swelling ratios of the materials are given in Figure 1e across a range of crosslink densities and chain lengths with 20% loading of either Neut or SMA polymer, with Figure S11a-b giving swelling ratios of HEA materials and materials with increasing Neut loadings. As anticipated, polymers with shorter chain lengths or lower crosslink densities showed higher swelling ratios. Swelling of Neutfunctionalized materials was comparable to 100/6 HEA. Evolution of typical swelling ratio over time is given in Figure S12. Both the unfunctionalized and functionalized materials became more brittle after being allowed to swell for several hours. However, the functionalized materials were substantially more fragile in the swollen state than the unfunctionalized poly(HEA) network polymers. This brittleness after extended swelling suggests that the polymer networks are best used in applications where they may be in moist environments or exposed to aqueous media for relatively short times.

The surface morphology of the polymers was studied using SEM (Figure S13). Both low magnification (100x) and high magnification (4.5Kx) images were captured to illustrate the differences in texture between samples. At low magnification, some samples show flakes (a, b, j) or debris like features (c, d, e, g) while others appear smooth (f, i, o). At high magnification the larger features become less prominent and striations (a, b), ripples (f, g, o), and wrinkles (e, l, m) can be seen on the surface. All samples were coated in 20 nm of gold for conductivity.

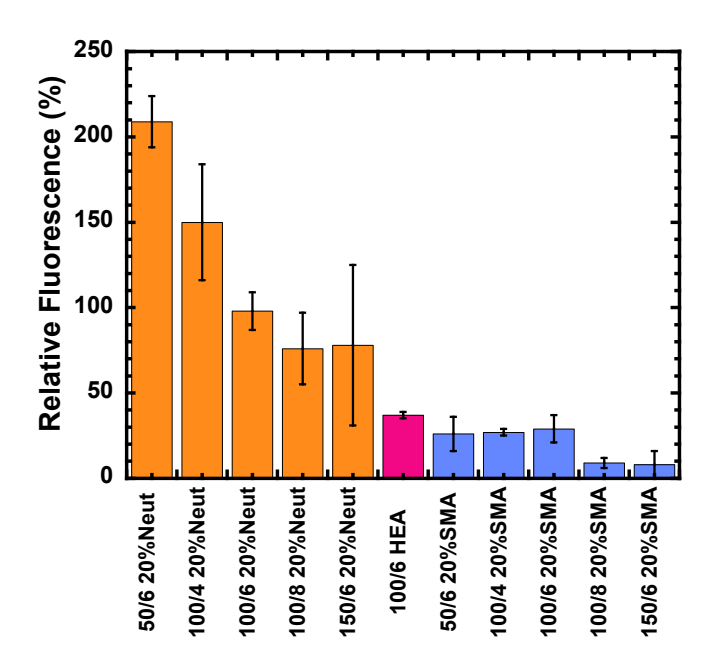


Figure 2. Liposome disruption performance as a function of varying chain length, crosslinker density, and type of functional polymer (orange – materials containing Neut-SH; blue – materials containing SMA-SH). For network polymers, liposomes solution was added to the network polymer at a 5%w/v ratio. All samples were inverted 10 times over the course of 80 sec. For all figures, fluorescence is normalized between a positive control (10% triton solution) at 100% and the completely undisturbed liposomes as the negative control at 0%.

With mechanically robust materials in hand, membrane disruption activity of soluble and network materials was assessed. Prior to this assessment, we confirmed the stability of dilute liposome solution by inverting the solution in absence of network materials. The fluorescence of diluted liposome solution after 10 rotations showed no significant difference with the negative control (Figure S14). The fluorescence properties of the polymers SMA-SH and Neut-SH polymers were also evaluated (Figure S15), with the soluble polymers having essentially no fluorescence. In our membrane disruption assay, we observed that the soluble SMA-SH, as expected, rapidly disrupts

the liposomes (Figure S16), with activity comparable to the traditional detergent Triton X-100. Soluble Neut-SH was somewhat less effective compared to SMA-SH or the Triton control. Figure S17 shows the amount of material required to achieve consistently high performance. The materials composed of 10% Neut-SH performed with high variability. Consistent performance was observed for 20% and 40% Neut, and with similar activities, 20% Neut or SMA was chosen as the composition for investigating the effects of chain length and crosslinker density. Importantly, the materials disrupt lipid vesicles very quickly (Figure S17), typically in less than 1 minute, which is substantially faster than the swelling of the network (Figure S12). The 20% and 40% Neut materials showed relative fluorescence at 0 inversion, probably due to their own bilayer disruptive properties since, the diluted liposome solution didn't show any mechanical disruption upon rotation as seen in Figure S14. However, by just 4 full rotations (about 30 seconds), the 20% and 40% Neut materials reach total liposome disruption and fluorophore release. If applied to a highcontact surface, it is likely that all membranes would be dismantled between uses, especially when one considers that the mass ratio is reversed in a real-world scenario. Here, the liposome solution is \sim 95% of the mass, while the functional polymer is \sim 1% of the mass. In the field, the functional polymer would be the bulk material and respiratory droplets would be comparatively small. Contact angles and dynamic light scattering data were also taken for these SMA-SH and Neut-SH polymers (Figure S18 and S19). The contact angle measurements show a substantial reduction in contact angle against the hydrophobic surface of polystyrene across all concentrations tested. The dynamic light scattering was consistent with very small objects of ca. 10 nm with no visible light scattering, consistent with limited polymer aggregation.

Having established potential for rapid lipid-bilayer disruption by these materials, it is important to screen performance against network parameters such as primary chain length or crosslink density. However, as seen in Figure 2 the bilayer disrupting performance is

essentially reversed in the network materials. SMA materials caused insubstantial fluorescence increases, performing as well or worse than the unfunctionalized HEA network. The Neut materials performed very well, reaching or exceeding the fluorescence of the Triton X-100 positive control. It is possible to exceed the performance of the Triton X-100 positive control due to kinetic factors. If the SMA or Neut-based material leads to faster disruption, it is possible to disrupt more lipid vesicles in the 10 rotations of the disruption assay, compared to the Triton X-100.

The poor performance of SMA in the solid state was notable given its superior solution performance. This could be due to differences in how the fully anionic SMA polymer arranges within the in the solid state material compared to its solution conformation. Due to the anionic charge the polymer likely exists in a specific conformation in the solid state with counterions present to balance charge. In contrast, a zwitterionic polymer like Neut-SH, the polymer is likely to have a less restricted state than the fully anionic SMA-SH. Additionally, initial investigation found that SMA-SH with a 1:1 styrene:maleic anhydride ratio (lacking a styrene block) was unable to disrupt lipid vesicles even in solution. If the critical tail-end of the polymer is anchored to the network of hydrophilic HEA, insertion and membrane disintegration could be inhibited, contributing to the poor performance of SMA-based materials in disrupting lipid-bilayers.

Some clear trends emerge in Figure 2 regarding chain length and crosslinker density, which both determine the stiffness of the network. We hypothesized that stiffer networks would exhibit inferior performance due to either poor flexibility of the functional polymer, or smaller pore size that reduces accessible surface area. Indeed, the looser networks (50/6% and 100/4%) perform better than their stiff counterparts (150/6% and 100/8%). Indeed, the

data in Figure 2 closely follows the trends in swelling ratios in Figure 1e. The overall highest disruption performance comes from the 50/6% Neut materials.

Material stiffness appears to correlate with disruption performance. Some mechanistic insights can be gleaned from the trends. It is believed that the activity of SMA and its relatives involves the cooperation of many polymer chains.⁶⁹ Adoption of liposome-breaking conformations must be entropically unfavorable when all participating polymers are covalently anchored to a network and must converge around a single point. Thus, it possible that more flexible and mobile network (i.e., lower Young's modulus and higher swelling ratio) allows for functional polymers to easily access conformations that allow for cooperative action against liposomes or other lipid based nanoparticles.

Regarding pore size, it is notable that the 50/6 20% Neut performs better than the 100/4 20% Neut material, despite the two having similar Young's moduli (Figure 1b-c). Assuming complete formation of elastically effective crosslinks, the 50/6% materials should have smaller pore sizes than the 100/4% materials due to increased crosslinker density and thus lower average distance between two crosslinks. However, the superior performance of the 50/6 materials than in the 100/4 network can be rationalized by the higher swelling ratio of the 50/6 materials containing 20% Neut polymer.

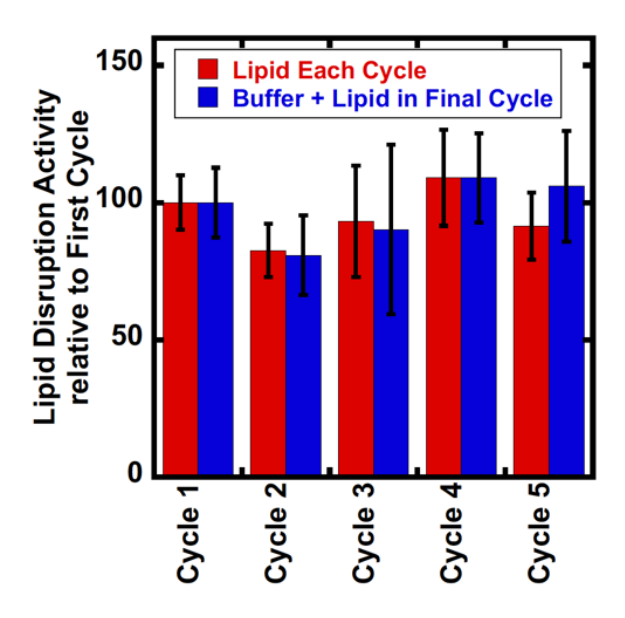


Figure 3. 50/6 20%Neut (the highest-performing material in the chain length/crosslinker series) were pretreated with either buffer (blue) or a 1% solution of MLVs (red) followed by liposome disruption assay in the final cycle. Fluorescence is normalized between a positive control (10% triton solution) at 100% and the complete undisturbed liposomes as the negative control at 0%.

The problem of fouling is also a concern for self-disinfecting materials. Proteins and lipids can irreversibly bind to a surface and thus passivate it. An ideal surface continues to function after being saturated with biomass. Figure 3 investigates whether previous saturation with lipids affects the function of these materials. Since the materials are preswollen, in this case the positive (10%-Triton) and negative control of an unperturbed system are also included in Figure 2 rather than showing relative activity. It was possible that pre-hydrated material would perform better than dry material, so there was a set of buffer-soaked control samples in addition to the samples pre-soaked with the lipid solution. In both cases, performance is comparable to or slightly higher than disruption by dry material, and both are superior to the Triton solution. As seen in Figure 3, prior exposure

to lipids had essentially no impact on the performance of the material studied over five cycles, suggesting that the materials could be reused for repeated lipid-bilayer disruption performance. The consistent performance in the 50/6 20%Neut material over 5 cycles demonstrated in Figure 3 also suggests that minimal Neut polymer leaches out in each assay. This is because if substantial amounts of the Neut polymer were released from the material in the first or second cycle, there would be substantially less polymer available for subsequent lipid-bilayer disruption cycles.

The capacity of these polymers to bind the Spike protein of SARS-CoV-2 was also investigated in Figure 4a-b. Host cell receptor binding domain (HCRBD) of SARS-CoV-2 spike protein was incubated with 100/6 materials to assay binding affinity. Interestingly, unfunctionalized HEA binds around 90% of the HCRBD. 100/6 20% Neut performs similarly, while 100/6 20% SMA binds around 70% of protein, making it inferior for both protein binding and membrane disruption in the solid state. Reusability of network materials were also investigated, which showed almost similar trend of spike protein capture in three consecutive cycles (Figure S20).

Finally, refocusing on the application of these materials, the adhesive properties were investigated in Figure 4c and 4d. These materials are unlikely to be used as bulk materials but instead they should adhere to a variety of existing surfaces if they are to be adapted for use in everyday high contact surfaces, potentially reducing fomite-based disease transmission. Additionally, to address airborne diseases, the adhesion to various filter-like surfaces was also investigated. In these modified filter systems, viruses in respiratory droplets making contact with such filtration surfaces could be inactivated and thus recirculated air would be cleaned if passed through a filter equipped with these polymers. Materials with disulfide linkages are known to have adhesive properties at elevated

temperatures.^{71,72} Good adhesive properties were observed in 100/6 20% Neut materials at room temperature with a variety of surfaces including both surgical and KN95 face masks.

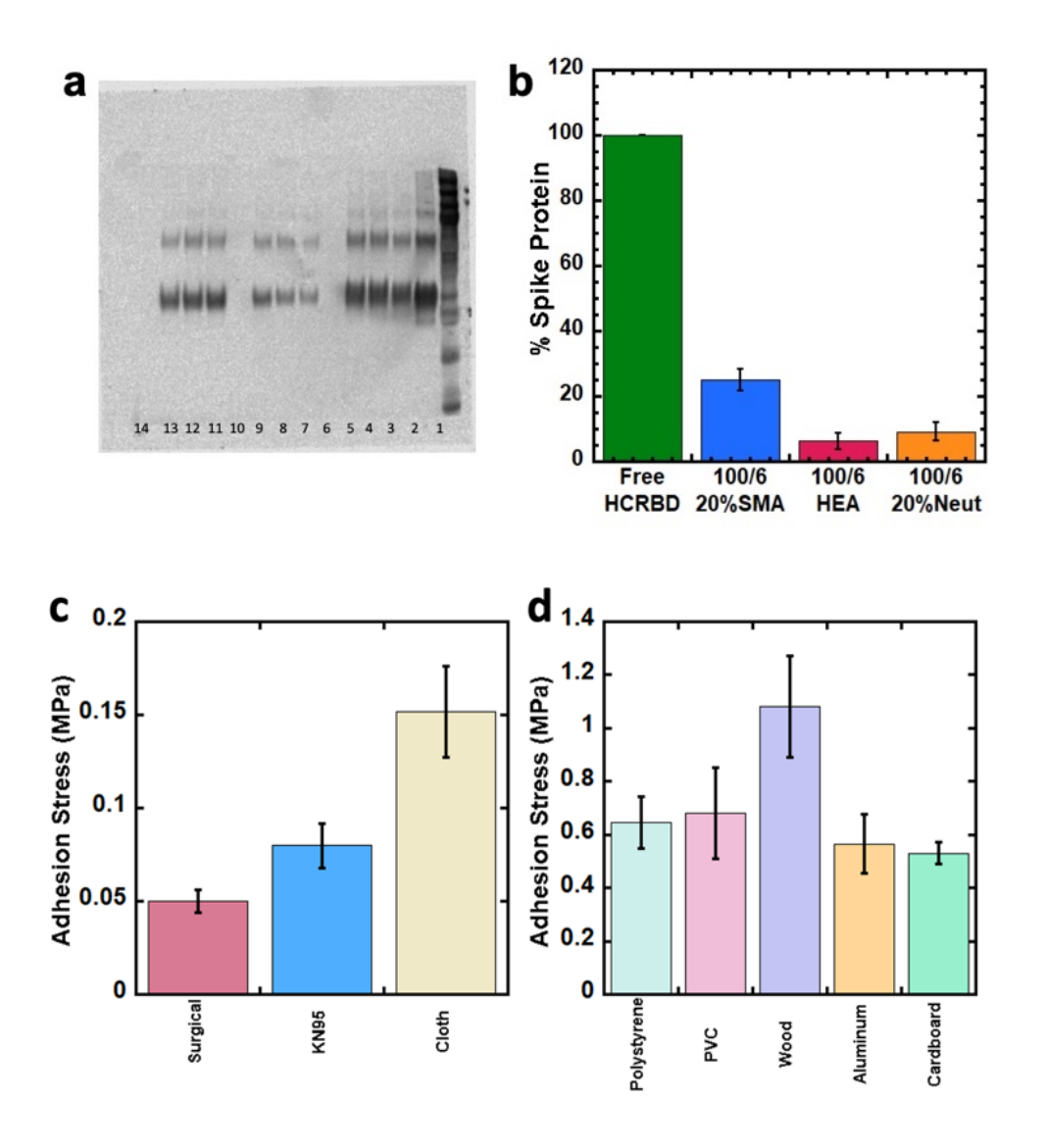


Figure 4. a-b) Spike protein capture by network materials. The soluble domain of spike protein (HCRBD) was incubated with network materials and then assayed by Western blot. (a) Western blot image of recovered HCRBD. Lanes: 1. Ladder 2. HCRBD (free protein control) (0.14mg/mL) 3-5. HCRBD (0.14mg/mL) treated with 100/6 20% SMA. 6. Buffer treated with 100/6 20% SMA. 7-9. HCRBD (0.14mg/mL) treated with 100/6% HEA. 10. Buffer treated with 100/6 HEA. 11-13. HCRBD (0.14mg/mL) treated with 100/6 20% Neut. 14. Buffer treated with 100/6 20% Neut. (b)

Analysis of Western blot band intensities relative to control. Error bars are for the 3 lanes shown for each network polymer. c-d) Adhesive properties of 100/6 20%Neut samples c). With polypropylene surgical or KN95 masks, and cloth masks, d). With polystyrene, PVC, wood, aluminum, and cardboard strips

To determine the functional application of these network materials, KN95 and surgical masks were coated with 50/6 20% Neut (the highest-performing material in the chain length/crosslinker series) in two different concentrations, 2.5 mg/cm², and 5 mg/cm². This loading of material leads to a very thin layer of functional polymer network on the surface of the masks. Due to this very thin layer of functional polymer, combined with the Young's modulus in the order of MPa, consistent with a rubbery material,⁷³ leads to flexible modified masks, which can easily be contoured to match the shape of the user's face. Figure 5 demonstrates the lipid-bilayer disrupting activity of the coated masks. As seen in Figure 5, coating a KN95 mask with 50/6 20%Neut at 2.5 and 5.0 mg/cm² resulted in 53% and 115% 61% liposome disruption, respectively. Similarly coating a surgical mask at 2.5 and 5 mg/cm² of the 50/6 20%Neut led to 61% and 121% liposome disruption, respectively. In all cases the relative lipid bilyaer disruption is referenced to 10% triton. We also evaluated the pressure drop and filtration efficiency of the coated masks. The pressure drop test showed a similar response for the coated mask to uncoated masks (Figure S21a-b). Coating KN95 and surgical masks exhibited insignificant differences in filtering glycerin droplets (Figure S22a-d).

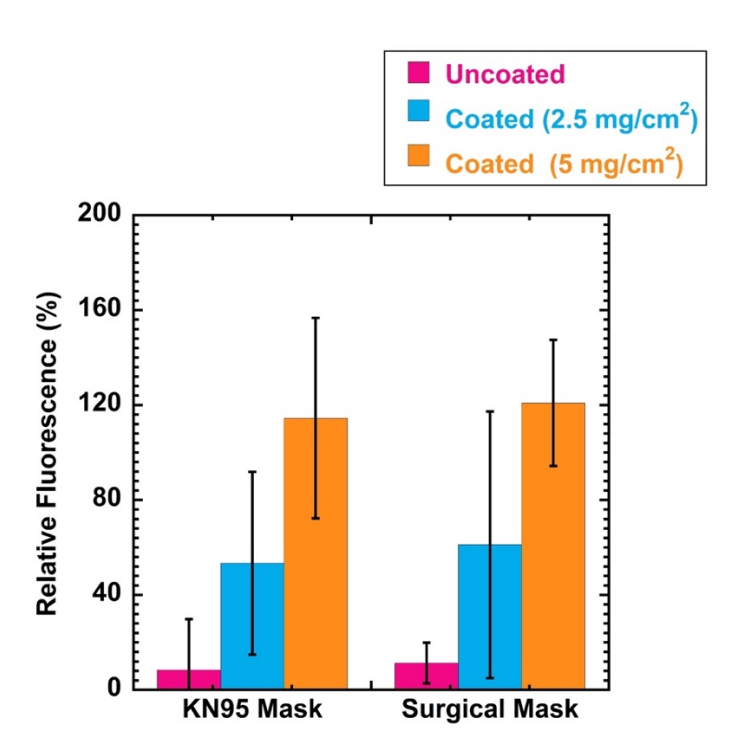


Figure 5. Liposome disruption performance of 50/6 20% Neut (the highest-performing material in the chain/crosslinker series) coated KN95 and surgical masks. Each type of masks was coated in two different concentrations 2.5 mg/cm² and 5 mg/cm². Fluorescence is normalized between a positive control (10% triton solution) at 100% and the completely undisturbed liposomes as the negative control at 0%.

Conclusions

A series of mechanically sound materials incorporating different macromolecular SMA based lipid-bilayer disrupting materials were synthesized. These materials have the ability to disrupt lipid-bilayer membranes in which the liposomal membrane is intended to mimic the viral envelope. The polymer's primary chain length, crosslinker densities and loading of the bilayer disrupting polymer could be controlled independently. Timescales of disruption are fast – with complete dye leakage and lipid-bilayer disruption possible in under one minute. The best performing material for liposome disruption was the 50/6 20% Neut. These materials also have the potential to capture soluble fragments of the SARS-

CoV-2 spike protein. Finally, the materials adhere well to a range of bulk and filter materials. Masks coated with the polymer material retains permeability while gaining lipid-bilayer disruption potential.

Author Contributions

RCP and DK were involved in conceptualization. KMB, MSR, NDAW, EG, MZS, BMC were involved in investigation and performing experiments. All authors were involved in formal analysis, writing and editing.

Conflicts of interest

There are no conflicts to declare.

Acknowledgements

We thank Dr D. Steven Keller for assistance with contact angle measurements. This work was supported by the National Science Foundation under Grant No. (DMR-2030567) to DK and RCP. GAL would like to acknowledge support, NIGMS/NIH Maximizing Investigator's Research Award (MIRA) R35 GM126935 award. 400 MHz NMR instrumentation is supported through funding from the National Science Foundation under grant number (CHE-1919850). DK acknowledges support from Miami University through the Robert H. and Nancy J, Blayney Professorship. RCP acknowledges support from Miami University through the Ernst H. Volwiler Professorship.

Notes and references

- S. B. DUFF, E. A. SCOTT, M. S. MAFILIOS, E. C. TODD, L. R. KRILOV, A. M. GEDDES and S. J. ACKERMAN, *Journal of Food Protection*, 2003, **66**, 2103–2115.
- N. Goodyear, N. Brouillette, K. Tenaglia, R. Gore and J. Marshall, *Journal of Applied Microbiology*, 2015, **119**, 1245–1252.
- J. S. Greatorex, R. F. Page, M. D. Curran, P. Digard, J. E. Enstone, T. Wreghitt, P. P. Powell, D. W. Sexton, R. Vivancos and J. S. Nguyen-Van-Tam, *PLoS ONE*, 2010, **5**, e8987.
- G. Kampf, D. Todt, S. Pfaender and E. Steinmann, *Journal of Hospital Infection*, 2020, **104**, 246–251.
- A. Kapur, C. Baldwin, M. Swanson, N. Wilberforce, G. McClenachan and M. Rentschler, *The International Journal of Life Cycle Assessment*, 2012, **17**, 377–387.
- 6 S. A. Boone and C. P. Gerba, *Appl. Environ. Microbiol.*, 2007, **73**, 1687–1696.
- L. Setti, F. Passarini, G. De Gennaro, P. Barbieri, M. G. Perrone, M. Borelli, J. Palmisani, A. Di Gilio, V. Torboli, F. Fontana, L. Clemente, A. Pallavicini, M. Ruscio, P. Piscitelli and A. Miani, *Environmental Research*, 2020, **188**, 109754.
- 8 R. Zhang, Y. Li, A. L. Zhang, Y. Wang and M. J. Molina, *Proceedings of the National Academy of Sciences*, 2020, **117**, 14857–14863.
- 9 G. A. Somsen, C. van Rijn, S. Kooij, R. A. Bem and D. Bonn, *The Lancet Respiratory Medicine*, 2020, **8**, 658–659.
- S. Vardoulakis, M. Sheel, A. Lal and D. Gray, *Australian and New Zealand Journal of Public Health*, 2020, **44**, 333–335.
- 11 N. Castaño, S. C. Cordts, M. Kurosu Jalil, K. S. Zhang, S. Koppaka, A. D. Bick, R. Paul and S. K. Y. Tang, *ACS Omega*, 2021, **6**, 6509–6527.
- M. M. Querido, L. Aguiar, P. Neves, C. C. Pereira and J. P. Teixeira, *Colloids and Surfaces B: Biointerfaces*, 2019, **178**, 8–21.
- 13 S.-D. Walji and M. G. Aucoin, *American Journal of Infection Control*, 2020, **48**, 1255–1260.
- S. M. Barbon, N. P. Truong, A. G. Elliott, M. A. Cooper, T. P. Davis, M. R. Whittaker, C. J. Hawker and A. Anastasaki, *Polymer Chemistry*, 2020, **11**, 84–90.
- P. R. Judzewitsch, T.-K. Nguyen, S. Shanmugam, E. H. H. Wong and C. Boyer, *Angewandte Chemie International Edition*, 2018, **57**, 4559–4564.
- S. Ghosh, R. Mukherjee, D. Basak and J. Haldar, *ACS Applied Materials & Interfaces*, 2020, **12**, 27853–27865.
- 17 N. van Doremalen, T. Bushmaker, D. H. Morris, M. G. Holbrook, A. Gamble, B. N. Williamson, A. Tamin, J. L. Harcourt, N. J. Thornburg, S. I. Gerber, J. O. Lloyd-Smith, E. de Wit and V. J. Munster, *New England Journal of Medicine*, 2020, **382**, 1564–1567.
- 18 W. Sim, R. Barnard, M. A. T. Blaskovich and Z. Ziora, *Antibiotics*, 2018, **7**, 93.
- 19 A. E. Madkour and G. N. Tew, *Polymer International*, 2008, **57**, 6–10.
- 20 J. C. Tiller, 2010, pp. 193–217.
- 21 X. Si, X. Quan and Y. Wu, *Applied Microbiology and Biotechnology*, 2015, **99**, 10861–10870.
- 22 X. Xue, J. K. Ball, C. Alexander and M. R. Alexander, *Matter*, 2020, **3**, 1433–1441.
- 23 L. M. Pandey, Surface Eng., 2020, **36**, 901–907.
- J. Haldar, J. Chen, T. M. Tumpey, L. v Gubareva and A. M. Klibanov, *Biotechnol. Lett.*, 2008, **30**, 475–479.

- 25 H. B. B, Y. W. Sze, H. P. T, C. Jianzhu and K. A. M, *Proc. National Acad. Sci.*, 2011, **108**, 61–66.
- A. J. Blok, P. Gurnani, A. Xenopoulos, L. Burroughs, J. Duncan, R. A. Urbanowicz, T. Tsoleridis, H. Müller-Kräuter, T. Strecker, J. K. Ball, C. Alexander and M. R. Alexander, *Biointerphases*, 2020, **15**, 061005.
- 27 I. Mannelli, D. Janner, F. Sagués and R. Reigada, Environ. Chem., 2017, 14, 319–326.
- D. Park, A. M. Larson, A. M. Klibanov and Y. Wang, *Applied Biochemistry and Biotechnology*, 2013, **169**, 1134–1146.
- 29 J. Haldar, A. K. Weight and A. M. Klibanov, *Nature Protocols 2007 2:10*, 2007, **2**, 2412–2417.
- 30 B. B. Hsu, S. Y. Wong, P. T. Hammond, J. Chen and A. M. Klibanov, *Proc Natl Acad Sci U S A*, 2011, **108**, 61–66.
- M. Sorci, T. D. Fink, V. Sharma, S. Singh, R. Chen, B. L. Arduini, K. Dovidenko, C. L. Heldt, E. F. Palermo and R. H. Zha, *ACS Appl. Mater. Interfaces*, 2022, **14**, 25135–25146.
- A. M. Larson, B. B. Hsu, D. Rautaray, J. Haldar, J. Chen and A. M. Klibanov, *Biotechnology and Bioengineering*, 2011, **108**, 720–723.
- B. S. T. Peddinti, F. Scholle, M. G. Vargas, S. D. Smith, R. A. Ghiladi and R. J. Spontak, *Materials Horizons*, 2019, **6**, 2056–2062.
- P. De Somer, E. De Clercq, A. Billiau, E. Schonne and M. Claesen, J Virol, 1968, 2, 878–85.
- A. Nagaraja, M. D. Jalageri, Y. M. Puttaiahgowda, K. Raghava Reddy and A. V. Raghu, *Journal of Microbiological Methods*, 2019, **163**, 105650.
- 36 E. A. Ali, M. Eweis, S. Elkholy, M. N. Ismail and M. Elsabee, *Macromolecular Research*, 2018, **26**, 418–425.
- J.-H. Jeong, Y.-S. Byoun and Y.-S. Lee, *Reactive and Functional Polymers*, 2002, **50**, 257–263.
- 38 W. J. Cloete, L. Verwey and B. Klumperman, *European Polymer Journal*, 2013, **49**, 1080–1088.
- 39 K. M. Burridge, B. D. Harding, I. D. Sahu, M. M. Kearns, R. B. Stowe, M. T. Dolan, R. E. Edelmann, C. Dabney-Smith, R. C. Page, D. Konkolewicz and G. A. Lorigan, *Biomacromolecules*, 2020, **21**, 1274–1284.
- 40 M. Xue, L. Cheng, I. Faustino, W. Guo and S. J. Marrink, *Biophysical Journal*, 2018, **115**, 494–502.
- A. F. Craig, E. E. Clark, I. D. Sahu, R. Zhang, N. D. Frantz, M. S. Al-Abdul-Wahid, C. Dabney-Smith, D. Konkolewicz and G. A. Lorigan, *Biochimica et Biophysica Acta (BBA) Biomembranes*, 2016, **1858**, 2931–2939.
- J. M. Dörr, S. Scheidelaar, M. C. Koorengevel, J. J. Dominguez, M. Schäfer, C. A. van Walree and J. A. Killian, *European Biophysics Journal*, 2016, **45**, 3–21.
- 43 A. P. Bali, I. D. Sahu, A. F. Craig, E. E. Clark, K. M. Burridge, M. T. Dolan, C. Dabney-Smith, D. Konkolewicz and G. A. Lorigan, *Chemistry and Physics of Lipids*, , DOI:10.1016/j.chemphyslip.2019.02.003.
- B. D. Harding, G. Dixit, K. M. Burridge, I. D. Sahu, C. Dabney-Smith, R. E. Edelmann, D. Konkolewicz and G. A. Lorigan, *Chemistry and Physics of Lipids*, , DOI:10.1016/j.chemphyslip.2018.12.002.

- K. M. Burridge, B. D. Harding, I. D. Sahu, M. M. Kearns, R. B. Stowe, M. T. Dolan, R. E. Edelmann, C. Dabney-Smith, R. C. Page, D. Konkolewicz and G. A. Lorigan, *Biomacromolecules*, 2020, **21**, 1274–1284.
- 46 E. A. Ali, M. Eweis, S. Elkholy, M. N. Ismail and M. Elsabee, *Macromolecular Research*, 2018, **26**, 418–425.
- W. J. Cloete, L. Verwey and B. Klumperman, *European Polymer Journal*, 2013, **49**, 1080–1088.
- 48 A. Nagaraja, M. D. Jalageri, Y. M. Puttaiahgowda, K. Raghava Reddy and A. V. Raghu, *Journal of Microbiological Methods*, 2019, **163**, 105650.
- J.-H. Jeong, Y.-S. Byoun and Y.-S. Lee, *Reactive and Functional Polymers*, 2002, **50**, 257–263.
- 50 M.-Y. Wang, R. Zhao, L.-J. Gao, X.-F. Gao, D.-P. Wang and J.-M. Cao, *Frontiers in Cellular and Infection Microbiology*, , DOI:10.3389/fcimb.2020.587269.
- G. Moad, R. T. A. Mayadunne, E. Rizzardo, M. Skidmore and S. H. Thang, 2003, pp. 520–535.
- 52 S. Perrier, *Macromolecules*, 2017, 50, 7433–7447.
- P. J. Roth, D. Kessler, R. Zentel and P. Theato, *Macromolecules*, 2008, **41**, 8316–8319.
- 54 S. Z. Zard, *Macromolecules*, 2020, **53**, 8144–8159.
- 55 G. Moad and E. Rizzardo, *Polymer International*, 2020, **69**, 658–661.
- 56 M. Semsarilar and V. Abetz, *Macromolecular Chemistry and Physics*, 2021, **222**, 2000311.
- 57 S. Perrier and P. Takolpuckdee, *Journal of Polymer Science Part A: Polymer Chemistry*, 2005, **43**, 5347–5393.
- A. F. Craig, E. E. Clark, I. D. Sahu, R. Zhang, N. D. Frantz, M. S. Al-Abdul-Wahid, C. Dabney-Smith, D. Konkolewicz and G. A. Lorigan, *Biochimica et Biophysica Acta (BBA) Biomembranes*, 2016, **1858**, 2931–2939.
- P. R. Judzewitsch, T.-K. Nguyen, S. Shanmugam, E. H. H. Wong and C. Boyer, *Angewandte Chemie International Edition*, 2018, **57**, 4559–4564.
- J. A. Otter, C. Donskey, S. Yezli, S. Douthwaite, S. D. Goldenberg and D. J. Weber, *J. Hosp. Infect.*, 2016, **92**, 235–250.
- J. Barker, D. Stevens and S. F. Bloomfield, J. Appl. Microbiol., 2001, **91**, 7–21.
- J. Sills, K. A. Prather, L. C. Marr, R. T. Schooley, M. A. McDiarmid, M. E. Wilson and D. K. Milton, *Science* (1979), 2020, 370, 303–304.
- 63 H. Willcock and R. K. O'Reilly, *Polym. Chem.*, 2010, **1**, 149–157.
- J. R. Brender, D. L. Heyl, S. Samisetti, S. A. Kotler, J. M. Osborne, R. R. Pesaru and A. Ramamoorthy, *Physical Chemistry Chemical Physics*, 2013, **15**, 8908.
- 65 R. F. Chen and J. R. Knutson, *Analytical Biochemistry*, 1988, **172**, 61–77.
- 66 A. T. Coey, I. D. Sahu, T. S. Gunasekera, K. R. Troxel, J. M. Hawn, M. S. Swartz, M. R. Wickenheiser, R. Reid, R. C. Welch, C. G. Vanoye, C. Kang, C. R. Sanders and G. A. Lorigan, *Biochemistry*, 2011, **50**, 10851–10859.
- 67 R. B. Gennis, *Biomembranes : Molecular Structure and Function*, Springer New York, 1989.
- 68 B. Zhang, I. M. Jayalath, J. Ke, J. L. Sparks, C. S. Hartley and D. Konkolewicz, *Chem. Commun.*, 2019, **55**, 2086–2089.

- 69 M. Xue, L. Cheng, I. Faustino, W. Guo and S. J. Marrink, *Biophysical Journal*, 2018, **115**, 494–502.
- N. Peppas, European Journal of Pharmaceutics and Biopharmaceutics, 2000, **50**, 27–46.
- 71 U. Lafont, H. Van Zeijl and S. Van Der Zwaag, *ACS Appl Mater Interfaces*, 2012, **4**, 6280–6288.
- P. Carl, C. H. Kwok, G. Manderson, D. W. Speicher and D. E. Discher, *Proceedings of the National Academy of Sciences*, 2001, **98**, 1565–1570.
- 73 D. Koblar and M. Boltežar, *Exp. Tech.*, 2016, **40**, 235–244.

Table of Contents Entry

